

## Simulation tool for full-scale PRO systems using SWMMs

A. Ruiz-García<sup>a,\*</sup>, F. Tadeo<sup>b</sup>, I. Nuez<sup>a</sup>

<sup>a</sup> Department of Electronic Engineering and Automation, University of Las Palmas de Gran Canaria, Campus Universitario de Tafira, E-35017 Las Palmas de Gran Canaria, Spain

<sup>b</sup> Institute of Sustainable Processes, University of Valladolid, Spain

### HIGHLIGHTS

- Flexible simulation tool for full-scale PRO system design is proposed.
- Full-scale PRO system performance under different operating ranges.
- Users can set design parameters as permeability coefficients and spacer geometries.
- Safe operating windows and optimal operating points in full-scale PRO systems.

### ARTICLE INFO

#### Keywords:

Pressure retarded osmosis  
Energy generation  
Renewable energy  
Optimization  
Operating windows  
Power density  
Membranes

### ABSTRACT

Pressure retarded osmosis (PRO) is a process that is able to convert a salinity gradient into electrical energy through a turbine. This process has gained attention as a possible renewable energy technology for integration into desalination plants to improve their energy efficiency. Despite recent efforts, PRO is not yet commercially available due to drawbacks related to, among others, PRO membrane and module development. The aim of this study is to provide a simulation tool for full-scale PRO systems that allows accurate estimates of PRO-related energy generation to be made. The proposed tool enables analysis of single-stage systems with PRO modules in series and the setting of boundary conditions per module in terms of maximum flux recovery, and maximum and minimum feed/draw flow. The HTI OsMem™ 2521 spiral wound membrane module (SWMM) was evaluated considering an 8 in. diameter (high active area). Increasing the number of SWMMs in series was found to increase permeate flow and the energy that can be generated, even when considering the pressure drop on both draw and feed side and the effect of the dilution and concentration of the draw and feed solutions. The proposed tool allows to determine the safe operating windows and operating points for maximization of energy generation for fixed and variable operating conditions.

### 1. Introduction

The increased demand for accessible energy due to population growth and industrialization is one of the main concerns when considering climate change and greenhouse gas (GHG) emissions [1]. Most power systems are highly dependent on fossil fuels, which are limited resources and the main cause of GHG emissions and global warming [2]. Numerous technologies that could provide sustainable and efficient solutions for this energy issue are currently being studied. In this regard, one promising technology involves exploitation of the salinity gradient for the generation of energy [3,4]. In the last decade, membrane technologies for this type of energy generation, including battery mixing (BattMix), capacitive mixing (CapMix), forward osmosis-electrokinetic

(FO-EK), pressure retarded osmosis (PRO) and reverse electro dialysis (RED) methods, have been actively studied [5,6]. Of these technologies, PRO has proven to be the one with the highest efficiency and power density [7]. At the present time, the main challenge with PRO is to demonstrate its feasibility at pilot and full scale [8]. It has therefore been crucial to carry out PRO-related studies on, for example, improving membrane module properties, modeling [9,10], simulation and optimization of the process considering full-scale modules for practical operation [11,12], module configuration [13,14] and the effect of fouling on performance [15–19].

One of the main factors affecting full-scale PRO deployment concerns improvements to transport properties of the PRO membranes [20,21] in terms of the water permeability coefficient ( $A$ ) [22,23], the solute permeability coefficient ( $B$ ) [24] and the structural parameter ( $S$ )

\* Corresponding author.

E-mail addresses: [alejandroruiz@ulpgc.es](mailto:alejandroruiz@ulpgc.es) (A. Ruiz-García), [fernando.tadeo@uva.es](mailto:fernando.tadeo@uva.es) (F. Tadeo), [ignacio.nuez@ulpgc.es](mailto:ignacio.nuez@ulpgc.es) (I. Nuez).

<https://doi.org/10.1016/j.desal.2022.116025>

Received 26 April 2022; Received in revised form 20 July 2022; Accepted 30 July 2022

Available online 8 August 2022

0011-9164/© 2022 The Authors. Published by Elsevier B.V. This is an open access article under the CC BY license (<http://creativecommons.org/licenses/by/4.0/>).

Nomenclature	
<i>Acronyms</i>	
DS	Draw solution
ECP	External concentration polarization
ERD	Energy recovery device
FF	Fouling factor
FS	Feed solution
ICP	Internal concentration polarization
LCOE	Levelized cost of energy
PV	Pressure vessel
RES	Renewable energy sources
RO	Reverse osmosis
SOW	Safe operating window
SWMM	Spiral wound membrane module
SWRO	Seawater reverse osmosis
<i>Variables</i>	
$\dot{m}$	Mass flow ( $\text{kg s}^{-1}$ )
$A$	Water permeability coefficient ( $\text{m Pa}^{-1} \text{s}^{-1}$ )
$A_0$	Initial water permeability coefficient ( $\text{m Pa}^{-1} \text{s}^{-1}$ )
$B$	Solute permeability coefficient ( $\text{m s}^{-1}$ )
$CF$	Concentration factor
$C$	Concentration ( $\text{g L}^{-1}$ or $\text{kg (solute) kg}^{-1}$ (water))
$DF$	Dilution factor
$D$	Solute diffusivity ( $\text{m}^2 \text{s}^{-1}$ )
$d_h$	Hydraulic diameter of feed channel (m)
$H$	Feed-brine spacer height (m)
$h$	Specific enthalpy ( $\text{J kg}^{-1}$ )
$J$	Flux per unit area ( $\text{m}^3 \text{m}^{-2} \text{s}^{-1}$ )
$K$	Solute resistivity ( $\text{s m}^{-1}$ )
$k$	Mass transfer coefficient
$K_i$	Parameter applied to friction factor
$L$	Length of SWMM (m)
$n$	Number of SWMMs in PRO system
$P$	Power (W)
$p$	Pressure (Pa)
$P_{ew}$	Wall Peclet number
$Q$	Flow ( $\text{m}^3 \text{h}^{-1}$ or $\text{m}^3 \text{s}^{-1}$ )
$R$	Flux recovery (%)
$Sc$	Schmidt number
$Sh$	Sherwood number
$S_m$	Membrane surface ( $\text{m}^2$ )
$TCF$	Temperature correction factor
$T$	Temperature ( $^{\circ}\text{C}$ or $\text{K}$ )
<i>Greek letters</i>	
$\Delta p$	Pressure drop (Pa)
$\eta$	Performance
$\gamma$	Lumped parameter
$\mu$	Dynamic viscosity (Pa s)
$\nu$	Velocity ( $\text{m s}^{-1}$ )
$\pi$	Osmotic pressure (Pa)
$\rho$	Density ( $\text{kg m}^{-3}$ )
$\varepsilon$	Porosity in feed channel
<i>Subscripts</i>	
av	Average
D	Draw
F	Feed
id	Real
in	Input
m	Membrane
out	Output
p	Permeate
TB	Turbine

[25,26]. Currently, these properties for PRO membranes are in a range of  $1.58 \times 10^{-12}$ – $1.06 \times 10^{-11} \text{ m Pa}^{-1} \text{ s}^{-1}$  for  $A$ ,  $5.55 \times 10^{-9}$ – $6.11 \times 10^{-7} \text{ m s}^{-1}$  for  $B$  and 135–1374m for  $S$  [27]. Spacer geometry is another important factor in the performance of PRO membranes as it is related with the pressure drop ( $\Delta p$ ) and concentration polarization (CP) phenomena, as occurs in the reverse osmosis (RO) process [28]. Efforts have been made to study the effect of spacers and their optimization in PRO membranes [14,29,30]. Spacers impact on the mass transfer coefficients ( $k_D$  and  $k_F$  for the draw and feed side, respectively) given their relationship with velocity patterns on both the draw and feed side [31,32].

Y.C. Kim and M. Elimelech [33] assessed various scenarios for PRO osmotic power generation considering a salinity gradient range for the feed and draw solution (0.01–0.5 M as feed concentration ( $C_F$ ) and 0.5–2 M as draw concentration ( $C_D$ )). They also carried out a lab-scale experimental work of a proposed hybrid process of forward osmosis (FO) desalination and PRO power generation. It was concluded that high concentration brines paired with seawater could be used to exploit the salinity gradient when the performance of PRO membranes is improved. The need for low internal concentration polarization (ICP) effects and the capacity to withstand the high hydraulic pressures in PRO membranes have also been highlighted [34]. Some researchers have studied the PRO process as an energy generation system [35,36], and others as part of hybrid systems that include other membrane processes such as RO [37–41], FO [42–44] and membrane distillation [45,46]. However, very few studies have considered PRO systems at full scale, which is important to have a better forecast of their real-life performance.

In terms of full-scale modules and their applicability in real systems, there are some concerns related with membrane characteristics [47], fouling [48–51] and spacer designs [31]. Due to their operating

condition requirements, two main configurations are being promoted for the development of full-scale modules, spiral wound membrane modules (applied to flat-sheet membranes) [52] and hollow fiber (SWMMs and HF, respectively) [3,53]. With respect to PRO SWMMs, D. Attarde et al. [54] carried out a study with the HTI OsMem™ 2521 FO-CTA-MS-P-3H module that included experimental modeling and numerical parameter estimation. The influence of operating parameters such as draw flow in the input ( $Q_{D, in}$ ), draw concentration in the input ( $C_{D, in}$ ) and permeate flow ( $Q_p$ ) on power density ( $PD$ ) was assessed. As it was a small SWMM (diameter of 2.5 in. as opposed to the 8 in. diameter elements usually employed in the RO process), with  $0.5 \text{ m}^2$  as active surface ( $S_m$ ), the maximum  $Q_p$  value was  $7 \text{ L h}^{-1}$  for a  $C_{D, in} = 60 \text{ g L}^{-1}$  and  $C_{F, in} = 1 \text{ g L}^{-1}$ . Experimentally, the maximum value of  $PD$  for the aforementioned operating conditions was around  $1.1 \text{ W m}^{-2}$ , while when considering  $C_{D, in} = 30 \text{ g L}^{-1}$  the maximum value of  $PD$  was about  $0.57 \text{ W m}^{-2}$ . S. Lee et al. [55] performed a similar study using an 8040 PRO SWMM from Toray Chemical Korea Inc. This module has an  $S_m$  of  $17.9 \text{ m}^2$ . The maximum  $PD$  was around  $1.8 \text{ W m}^{-2}$  considering  $C_{D, in} = 35 \text{ g L}^{-1}$  and  $C_{F, in} = 0.14 \text{ g L}^{-1}$ . HF modules show a higher packing density than SWMMs, but are less popular in the RO process due to, among other reasons, a pH range of between 3 and 8, which hinders the efficiency of chemical cleaning in place. The main advantage of the HF membrane is the higher permeate production per module in comparison with SWMMs, which allows high recovery rates with just a few modules in series. G. O'Toole et al. [56] determined the net energy production from a simulated full-scale PRO system taking into consideration the efficiency of different components of the plant. The data of the PRO SWMM considered was taken from a previous study [57]. PV with one PRO SWMM disposed in series and in parallel were considered. After

optimizing the power gain, value of  $PD$  was  $3.25 \text{ W m}^{-2}$  and a permeate specific energy generation of  $0.42 \text{ kWh m}^{-3}$  was obtained considering PVs in series. M. Kishimoto et al. [9] carried out a simulation-based study to optimize power production by PRO using 2 HF modules of 5-inch scale (from TOYOBO) and seawater ( $C_{D, \text{in}} = 35 \text{ g L}^{-1}$ ) as the draw solution (DS) and pure water ( $C_{F, \text{in}} = 0 \text{ g L}^{-1}$ ) as the feed solution (FS). The pressure drop of both sides (using the Hagen-Poiseuille equation) and the change of concentrations were considered in this study. The two modules had  $S_m$  values of 70.5 and 65.6  $\text{m}^2$ , respectively.  $Q_{D, \text{in}}$  was in a range of 8–16  $\text{L min}^{-1}$  and  $Q_{F, \text{in}}$  between 8 and 12  $\text{L min}^{-1}$ . Results showed that the maximum power production was 104 W per module with a  $PD$  of  $1.58 \text{ W m}^{-2}$ . M. Higa et al. [58] also carried out an experimental study of an HF module from TOYOBO in a PRO process. An  $S_m$  of  $72 \text{ m}^2$  and  $C_{D, \text{in}} = 29.25 \text{ g L}^{-1}$  (0.5 M NaCl) and tap water as  $C_{F, \text{in}}$  were considered. They obtained a maximum  $PD$  of  $0.14 \text{ W m}^{-2}$ , reporting that this low result was due to the low  $A$  in comparison with other modules. An optimization study to maximize the energy extraction of a full-scale HF PRO module (5-in.) was done by Y. Chen et al. [59]. Four ranges of salinity were considered: 0.6 M–5 M NaCl and 1.2 M–5 M NaCl as  $C_{D, \text{in}}$ , and 0.02 M–0.6 M NaCl and 0.02 M–1.2 M NaCl as  $C_{F, \text{in}}$ . Four modules in series were considered, obtaining for the case of 5 M NaCl and 0.6 M NaCl as  $C_{D, \text{in}}$  and as  $C_{F, \text{in}}$  respectively, a  $PD$  above  $5 \text{ W m}^{-2}$  (optimum result for this case). The authors highlighted that the more modules in series the lower the  $PD$  but the higher the generated energy. K. Saito [60] performed a pilot plant test for power generation using eight 10-inch HF modules. A  $PD$  of  $4.4 \text{ W m}^{-2}$  was obtained with  $C_{D, \text{in}} = 1 \text{ M NaCl}$ . In term of costs, it has been estimated that PRO-generated energy in 2030 would be between 50 and 100  $\text{€ kWh}^{-1}$  [61]. Some studies have compared the levelized cost of energy (LCOE) and capacity factor of PRO with other low carbon energy sources, concluding that reductions in PRO component costs are unlikely to make PRO cost competitive with renewable energy technologies [62–64]. It should be mentioned that one of the advantages of energy generation by PRO, in comparison with other low carbon energy sources, is that energy generated on the basis of the salinity gradient is dispatchable as the energy source does not suffer important fluctuations like wind or solar energy.

In the event that PRO processes are implemented for either the direct generation of energy or in a hybrid process to increase energy efficiency, it would be at full scale. Usually, to obtain the desired  $Q_p$  various full-scale PRO modules have to be arranged in series [65,66]. In addition, as happens with full-scale RO modules, there are some boundary conditions (in terms of maximum  $Q_{D, \text{out}}$  and  $Q_{F, \text{in}}$  and minimum  $Q_{F, \text{out}}$ ) that should be set by the manufacturer and taken into consideration when full-scale PRO systems are operated or simulated. Considering full-scale PRO systems and boundary conditions could help to identify the weakest points of this technology and provide more realistic results.

The aim of this study is to provide a PRO process simulator to obtain simulation-based results of full-scale PRO systems considering boundary conditions and SWMMs (with the algorithm customizable for HF membranes). Single-stage PRO systems are assessed in terms of performance. By obtaining the safe operating windows (SOWs), the optimal operating points for different values of  $C_{D, \text{in}}$  and  $C_{F, \text{in}}$  are determined. Although PRO plants usually include pumps, pre-treatment and energy recovery devices (ERDs), only the turbine as energy generating element was considered in this study as it focuses on how the operating parameters affect PRO systems.

## 2. Material and methods

### 2.1. PRO SWMM characteristics

For the purpose of simulating the behavior of PRO SWMM 8-inch modules, the data of available modules were used. Of the two commercial SWMMs available (HTI OsMem™ 2521 and 8040 PRO from Toray), the Toray version would in principle be preferable since it is an

8-inch module. However, the information available in the literature about this module is limited, with no data on the height of the permeate spacer or the solute resistivity ( $K$ ) for determining the ICP effect. However, these data are available for the HTI OsMem™ 2521 module. In order to consider an 8-inch module of this type, an up-scaling was required. To do so, the membrane active surface ( $S_m$ ) was considered. Given that for the OsMem™ 2521 module the  $S_m$  is  $0.5 \text{ m}^2$ , the  $S_m$  for the hypothetical 8-inch OsMem™ module would be  $15.53 \text{ m}^2$ . The porosity of the draw ( $\epsilon_D$ ) and feed ( $\epsilon_F$ ) sides is not available, and so the values were taken from RO SWMMs [67]. The rest of the SWMM parameters, such as  $A$ ,  $B$ , height of draw ( $H_D$ ) and feed ( $H_F$ ) spacers and  $K$ , were taken from [54]. The characteristic parameters of the SWMM considered are summarized in Table 1.

### 2.2. Process modeling

In the PRO process, the transport phenomenon across a semi-permeable membrane is based on basic thermodynamics that describe the free energy released during the spontaneous mixing of the DS and the FS [68,69]. From that theory, it can be deduced that the permeate flux ( $J_p$ ) is the product of  $A$  and the driving force across the membrane [68] (Eq. (1)):

$$J_p = A(\Delta\pi - \Delta p) \quad (1)$$

where  $\Delta\pi$  is the osmotic pressure gradient and  $\Delta p$  the pressure gradient, both across the membrane. To obtain  $Q_p$ ,  $J_p$  was multiplied by  $S_m$ . To determine  $\Delta\pi$ , the concentration on the membrane surface on both the draw and feed side has to be estimated. For this purpose, the effect of external and internal concentration polarization (ECP and ICP, respectively) has to be considered (1) [70] (Fig. 1).

$$A = A_0 \cdot TCF \cdot FF \quad (2)$$

$$\Delta\pi = \pi_{D,m} - \pi_{F,m} \quad (3)$$

$$\pi = 3.805C^2 + 42.527C + 0.434 \quad (4)$$

where  $A_0$  is the initial value of  $A$ ,  $TCF$  the temperature correction factor (value of 1.0 at  $25^\circ\text{C}$ ) [71] and  $FF$  the fouling factor (value of 1.0 as membrane without fouling was considered).  $\pi_{D, m}$  and  $\pi_{F, m}$  are the osmotic pressure on the membrane surface on the draw and feed side, respectively. It should be mentioned that for estimation of the  $TCF$ , equations applied to the RO process were used as an approximation as the temperature effect on the PRO process was not evaluated in this study. Eq. (4) [72] was used to calculate osmotic pressure from a NaCl concentration ( $\text{mol L}^{-1}$ ). For the calculation of  $\pi_{D, m}$  and  $\pi_{F, m}$ ,  $C_{D, m}$  and  $C_{F, m}$  were used, respectively, in Eq. (4).

$$C_{D,m} = \left( C_{D,av} + \frac{J_s}{J_p} \right) e^{\frac{-J_p}{\epsilon_D}} - \frac{J_s}{J_p} \quad (5)$$

$$C_{F,m} = \left( C_{F,av} + \frac{J_s}{J_p} \right) e^{\frac{J_p}{\epsilon_F}} e^{KJ_p} - \frac{J_s}{J_p} \quad (6)$$

**Table 1**  
Characteristic parameters of the SWMM.

Parameter	Value
Height 1 pt. A ( $\text{m Pa}^{-1} \text{ s}^{-1}$ )	$1.76 \times 10^{-12}$
$B$ ( $\text{m s}^{-1}$ )	$1.18 \times 10^{-7}$
$S_m$ ( $\text{m}^2$ )	15.53
$L$ (m)	1.0
$H_D$ (m)	$1.1 \times 10^{-3}$
$H_F$ (m)	$1.5 \times 10^{-3}$
$\epsilon_D$	0.89
$\epsilon_F$	0.65
$K$ ( $\text{s m}^{-1}$ )	$3.38 \times 10^{-5}$

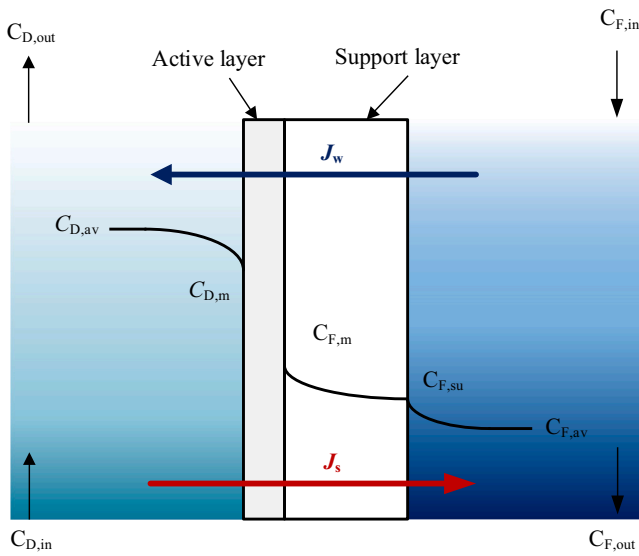


Fig. 1. Concentration profile of the membrane in PRO process considering ECP and ICP.

$$C_{D,av} = 0.5(C_{D,in} + C_{D,out}) \quad (7)$$

$$C_{F,av} = 0.5(C_{F,in} + C_{F,out}) \quad (8)$$

$$J_s = J_p \frac{B}{A\beta RT} \left( 1 + \frac{A\Delta p}{J_p} \right) \quad (9)$$

$$k_D = \frac{Sh_D D_{D,av}}{d_{h,D}} \quad (10)$$

$$k_F = \frac{Sh_F D_{F,av}}{d_{h,F}} \quad (11)$$

where  $C_{D,m}$  and  $C_{F,m}$  are the concentrations on the membrane surface on the draw and feed sides considering ECP and ICP [73,74],  $C_{D,av}$  and  $C_{F,av}$  are the average concentrations on the draw and feed side,  $J_s$  the reverse solute flux,  $k_D$  and  $k_F$  the mass transfer coefficients on the draw and feed side, and  $C_{D,in}$  and  $C_{D,out}$  are the input and output concentrations on the draw side.  $\beta$  is the dimensionless Van't Hoff factor for strong electrolytes ( $\beta = 2$  for NaCl) [72],  $R$  is the gas constant ( $8.31 \text{ J mol}^{-1} \text{ K}^{-1}$ ) and  $T$  is the absolute temperature (in K) of the solution, taken as  $25 < \text{circ}>C$  for both solutions (DS and FS) in this study. It should be noted that the proposed methodology is able to simulate PRO systems with different temperatures by considering  $T$  dependent equations for  $D$ ,  $\rho$  and  $\mu$ .  $Sh_D$  and  $Sh_F$  are the Sherwood numbers for the draw (dilutive) and feed (concentrate) [75],  $D_D$  and  $D_F$  are the diffusion coefficients of the DS and FS (using  $C_{D,av}$  and  $C_{F,av}$ , respectively, in Eq. (22), and  $d_{h,D}$  and  $d_{h,F}$  are the hydraulic diameters for the draw and feed side, respectively.  $Sh$  is a dimensionless number related with the ratio of convective to diffusive mass transport. Considering a laminar flow regime due to the low cross-flow rate used in this study,  $Sh_D$  and  $Sh_F$  can be estimated through Eqs. (12) and (13), respectively [75]:

$$Sh_D = 1.849 \left( Re_D Sc_D \frac{d_{h,D}}{L} \right)^{1/3} \left( 1.002 - 0.0319\gamma_D + 0.00034\gamma_D^2 - 0.001\gamma_D^3 \right) \quad (12)$$

$$Sh_F = 1.849 \left( Re_F Sc_F \frac{d_{h,F}}{L} \right)^{1/3} \left( 0.997 + 0.315\gamma_F + 0.022\gamma_F^2 - 0.008\gamma_F^3 \right) \quad (13)$$

$$\gamma_D = \frac{P_{ew,D}}{\left( Re_D Sc_D \frac{d_{h,D}}{L} \right)^{1/3}} \quad (14)$$

$$\gamma_F = \frac{P_{ew,F}}{\left( Re_F Sc_F \frac{d_{h,F}}{L} \right)^{1/3}} \quad (15)$$

$$P_{ew,D} = \frac{J_p d_{h,D}}{D_D} \quad (16)$$

$$P_{ew,F} = \frac{J_p d_{h,F}}{D_F} \quad (17)$$

$$Re_D = \frac{\rho_{D,av} \nu_{D,av} d_{h,D}}{\mu_{D,av}} \quad (18)$$

$$Re_F = \frac{\rho_{F,av} \nu_{F,av} d_{h,F}}{\mu_{F,av}} \quad (19)$$

$$Sc_D = \frac{\mu_{D,av}}{\rho_{D,av} D_D} \quad (20)$$

$$Sc_F = \frac{\mu_{F,av}}{\rho_{F,av} D_F} \quad (21)$$

$$D = -1.025 \times 10^{-10} C + 1.518 \times 10^{-9} \quad (22)$$

$$d_{h,D} = \frac{4\epsilon_D}{\frac{2}{H_D} + (1 - \epsilon_D) \frac{8}{H_D}} \quad (23)$$

$$d_{h,F} = \frac{4\epsilon_F}{\frac{2}{H_F} + (1 - \epsilon_F) \frac{8}{H_F}} \quad (24)$$

where  $\gamma_D$ ,  $\gamma_F$ ,  $P_{ew,D}$ ,  $P_{ew,F}$ ,  $Re_D$ ,  $Re_F$ ,  $Sc_D$ ,  $Sc_F$ ,  $\rho_{D,av}$ ,  $\rho_{F,av}$ ,  $\mu_{D,av}$  and  $\mu_{F,av}$  are, for each side respectively, a lumped parameter, wall Peclet number, Reynolds number, Schmidt number, solution density and dynamic viscosity.  $\rho$  and  $\mu$  were calculated for each solution (DS and FS) through Eqs. (25) and (26) with  $C_{D,av}$  and  $C_{F,av}$  in  $\text{mol L}^{-1}$ .

$$\rho = -1.047C^2 + 39.462C + 997.370 \quad (25)$$

$$\mu = 0.001(0.012C^2 + 0.065C + 0.985) \quad (26)$$

The term  $\Delta p$  (Eq. (1)) was calculated considering the pressure drop on both the draw and feed side.

$$\Delta p = p_{D,in} - \frac{PL_D}{2} - p_{F,in} + \frac{PL_F}{2} \quad (27)$$

$$PL_D = \lambda_D \cdot L \cdot \frac{\rho_D}{d_{h,D}} \cdot \frac{\nu_{D,av}^2}{2} \quad (28)$$

$$PL_F = \lambda_F \cdot L \cdot \frac{\rho_F}{d_{h,F}} \cdot \frac{\nu_{F,av}^2}{2} \quad (29)$$

$$\lambda_D = K_\lambda \cdot 6.23 Re_D^{-0.3} \quad (30)$$

$$\lambda_F = K_\lambda \cdot 6.23 Re_F^{-0.3} \quad (31)$$

where  $p_{D,in}$  and  $p_{F,in}$  are the input pressures on the draw and feed side,  $PL_D$  and  $PL_F$  are the pressure losses on the draw and feed side,  $L$  is the length of the membrane module and  $K_\lambda$  a parameter introduced by V. Geraldes et al. [76] to take into consideration additional pressure losses in the feed of the PVs and the SWMM fittings. Due to lack of information,  $K_\lambda$  was assumed to be the same for the draw and feed side. The concentrations in the output on both sides ( $C_{D,out}$  and  $C_{F,out}$ ) are affected by  $Q_p$  and  $J_s$ . The DS is diluted and the FS is concentrated due to both  $Q_p$

and  $J_s$ . The dilution and concentration factors ( $DF$  and  $CF$ ) due to  $Q_p$  are defined in Eqs. (32) and (33) respectively.

$$DF = \frac{C_{D,out}}{C_{D,in}} = \frac{1 - Y_m}{1} \quad (32)$$

$$CF = \frac{C_{F,out}}{C_{F,in}} = \frac{1}{1 - Y_m} \quad (33)$$

where  $C_{D,out}$  and  $C_{F,out}$  are the output concentrations due to only  $Q_p$  and  $Y_m$  is the recovery fraction of the SWMM ( $Q_p/Q_{F,in}$ ). The calculated  $R$  is  $Y_m$  in percentage. Mass fluxes (in  $kg\ s^{-1}$ ) in the DS and FS are shown in Eqs. (34) and (35):

$$C_{D,out}(Q_{D,in} + Q_p) = C_{D,in}DF(Q_{D,in} + Q_p) - J_s \quad (34)$$

$$C_{F,out}(Q_{F,in} - Q_p) = C_{F,in}CF(Q_{F,in} - Q_p) + J_s \quad (35)$$

### 2.3. Simulation procedure

All the above equations were used in an algorithm that simulates full-scale PRO systems (Fig. 2). The algorithm was implemented in MATLAB® and comprises three parts. The first part, named Stage (Fig. 2a), considers the boundary conditions in terms of  $Q_{f,max}$ ,  $Q_{D,max}$ ,  $Q_{f,min}$  and  $Q_{D,min}$ . Usually, in RO processes there are also constraints in terms of the maximum fraction recovery and maximum permeate flow per module. However, these two constraints were not taken into consideration, allowing PRO membrane modules to have higher recovery ratios than RO modules. Operating ranges per PV were also implemented:  $Q_{D,in}$  and  $Q_{F,in}$  from 3 to 16  $m^3\ h^{-1}$  in steps of 0.1  $m^3\ h^{-1}$ ;  $C_{D,in}$  from 30 to 60 g

$L^{-1}$  in steps of 10  $g\ L^{-1}$  and  $C_{F,in}$  from 0.5 to 3 in steps of 0.5  $g\ L^{-1}$ ; and  $p_{D,in}$  from 1 to a value that depended on  $C_{D,in}$  and  $p_{F,in}$  from 2 to 5 bar, both in steps of 0.5 bar. In order to obtain the Stage results, it is necessary to calculate the results per SWMM, and so the Module function (Fig. 2b) is called, providing an initial value of  $Y_m$ . This function is called by Stage using the MATLAB® optimizing function `fminbnd` [77,78] to find the minimum quadratic error on a bounded interval.

In the Module function, Eqs. (1)–(30) are calculated. For this purpose, the DS and FS output concentrations must be known. As these concentrations cannot be calculated directly as  $Y_e$  is needed, the `Concentrations_out` function is called (Fig. 2c). This function uses the estimated  $Y_e$  and Eqs. (32)–(35). With the estimated parameters  $Y_m$ ,  $C_{D,out}$  and  $C_{F,out}$ ,  $J_s$  is calculated from Eq. (9). Once  $J_s$  has been calculated,  $C_{D,out}$  and  $C_{F,out}$  are calculated from Eqs. (34) and (35) and the quadratic error for both concentrations can be calculated and minimized using the MATLAB® optimizing function `fminsearch`. Once the parameters of a module have been calculated, the values are stored and the Stage function repeats the procedure for the next module in series using the outputs of the first module as inputs for the second module and so on until 8 SWMMs in series are completed and as long as the established constraints are met.

### 2.4. Energy assessment

In order to calculate the energy generation potential of the full-scale PRO system, the specific enthalpy ( $h$ ) in the input and output of the turbine needs to be known. Fig. 3 shows the usual devices included in a PRO plant, the draw and feed pump, ERDs (pressure exchanger and booster pump) and turbine. The energy consumed by the draw and feed

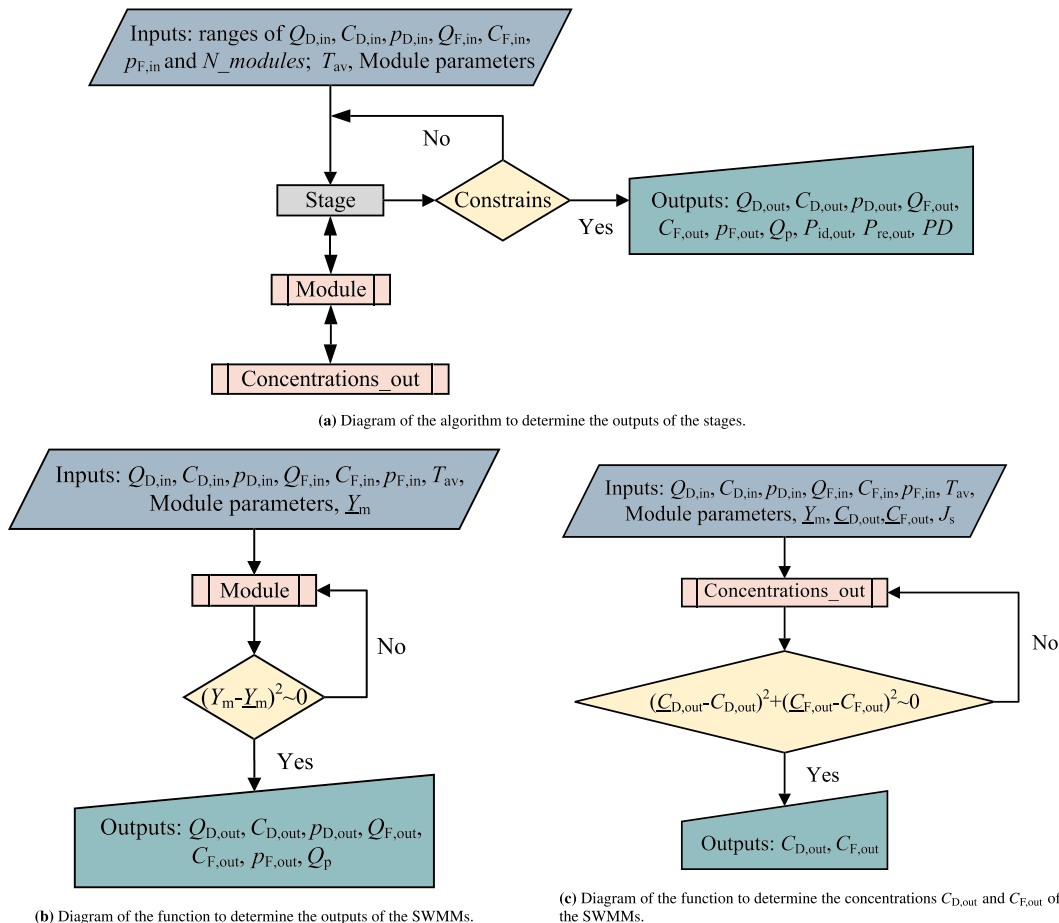


Fig. 2. Diagrams of the PRO simulator algorithms.

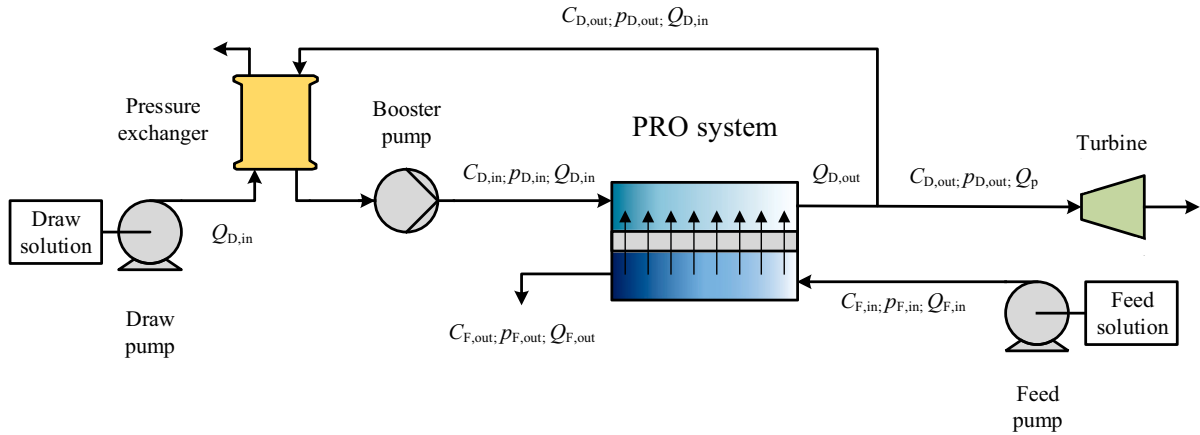


Fig. 3. Flow diagram of the PRO plant.

pump and ERDs were not considered. It should be note that the  $h$  of seawater is lower than that of pure water since the heat capacity of seawater is also lower than that of pure water. According with the data extracted from the seawater Gibbs energy function of International association for the properties of water and steam (IAPW) [79], Eqs. (36)–(38) can be used for the determination of  $h$  [80]. For a pressure other than atmospheric pressure ( $p_0$ ), specific enthalpy ( $h(T, p, C)$ ) can be calculated through Eq. (38). From the results of the PRO systems, the ideal power output ( $GP_{id}$ ) and power density ( $PD_{id}$ ) are calculated through Eqs. (39), (40) and (41) respectively.

$$h(T, p_0, C) = h_w - C(b_1 + b_2w_s + b_3w_s^2 + b_4w_s^3 + b_5T + b_6T^2 + b_7T^3 + b_8w_sT + b_9w_s^2T + b_{10}w_sT^2) \quad (36)$$

$$h_w = 141.355 + 4202.070T - 0.535T^2 + 0.004T^3 \quad (37)$$

$$\begin{aligned} b_1 &= -2.348 \times 10^4, b_2 = 3.152 \times 10^5, b_3 = 2.803 \times 10^6 \\ b_4 &= -1.446 \times 10^7, b_5 = 7.826 \times 10^3, b_6 = -4.417 \times 10^1 \\ b_7 &= 2.139 \times 10^{-1}, b_8 = -1.991 \times 10^4, b_9 = 2.778 \times 10^4 \\ b_{10} &= 9.728 \times 10^1 \end{aligned} \quad (38)$$

$$h(T, p, C) = h(T, p_0, C) + \vartheta(p - p_0)$$

where  $\vartheta$  is the specific volume which is the reverse of  $\rho$ .  $\vartheta$  was calculated for both the DS and FS using the  $\rho$  of each solution in the input and output of the devices considered.

$$P_{TB} = \eta_{TB} \dot{m}_{TB} (h_{TB,in} - h_{TB,out}) \quad (39)$$

$$\dot{m}_{TB} = Q_p \rho_{D,out} \quad (40)$$

$$PD_{id} = \frac{P_{TB}}{nS_m} \quad (41)$$

where  $\eta_{TB}$  is the performance of the turbine and  $n$  the number of SWMMs in the PRO system.

### 3. Results and discussion

#### 3.1. Impact of $C_{F, in}$

Figs. 4 and 5 show the maximum power density ( $PD_{id, max}$ ) and maximum power in the turbine ( $P_{TB, max}$ ) in a PRO system with 1 to 8 SWMMs in series,  $C_{D, in} = 30 \text{ g L}^{-1}$  and  $p_{F, in} = 2 \text{ bar}$ . Fig. 4 shows the results for  $C_{F, in} = 0.5 \text{ g L}^{-1}$  and Fig. 5 the results for  $C_{F, in} = 2.5 \text{ g L}^{-1}$ . It can be seen that  $PD_{id, max}$  was reached with 3 SWMMs in series, but the more SWMMs in series the more energy could be generated in the turbine. For values of  $C_{D, in} = 30 \text{ g L}^{-1}$  and  $p_{F, in} = 2 \text{ bar}$ , an increment of 2

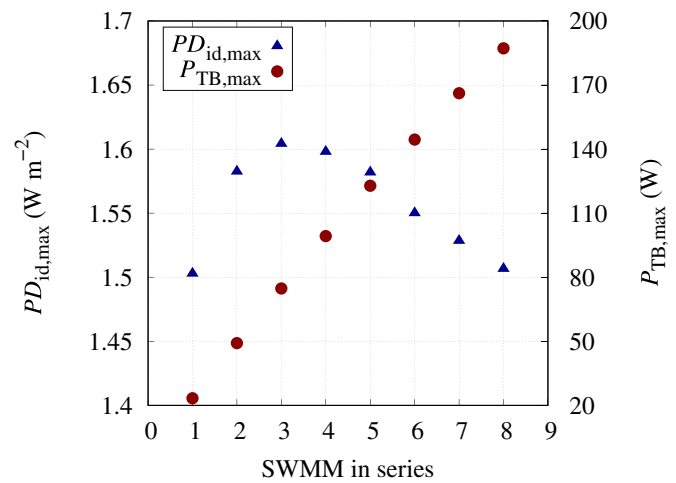


Fig. 4.  $PD_{id, max}$  and  $P_{TB, max}$  for 1 to 8 SWMMs in series,  $C_{D, in} = 30 \text{ g L}^{-1}$ ,  $C_{F, in} = 0.5 \text{ g L}^{-1}$  and  $p_{F, in} = 2 \text{ bar}$ .

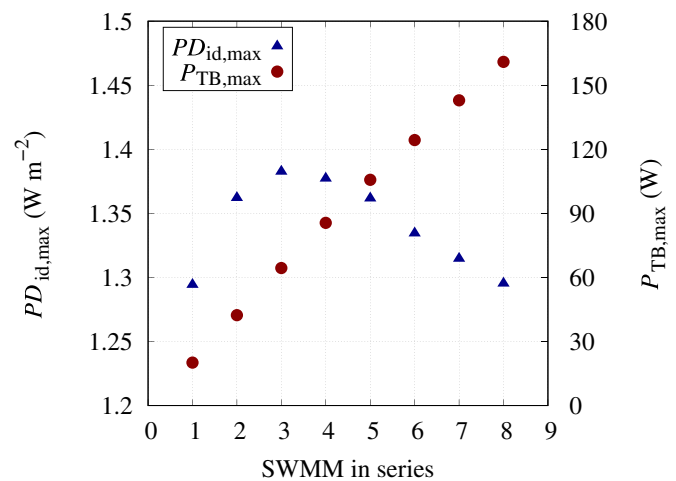


Fig. 5.  $PD_{id, max}$  and  $P_{TB, max}$  for 1 to 8 SWMMs in series,  $C_{D, in} = 30 \text{ g L}^{-1}$ ,  $C_{F, in} = 2.5 \text{ g L}^{-1}$  and  $p_{F, in} = 2 \text{ bar}$ .

$\text{g L}^{-1}$  in the  $C_{F, in}$  causes decreases of about  $0.22 \text{ W m}^{-2}$  and  $26 \text{ W}$  for  $PD_{id, max}$  and  $P_{TB, max}$ , respectively. This difference increases slightly with the increase of  $p_{F, in}$  and  $C_{D, in}$ . For values of  $C_{D, in} = 40 \text{ g L}^{-1}$  and  $p_{F, in} = 2 \text{ bar}$ , an increment of  $2 \text{ g L}^{-1}$  in the  $C_{F, in}$  causes a decrease of

about 0.28 W m<sup>-2</sup> for  $PD_{id, max}$  and 33 W for  $P_{TB, max}$ . Depending on the feedwater source, its salinity could vary and is an important factor to take into consideration. The operating points to have  $PD_{id, max}$  and  $P_{TB, max}$  are the same (Tables 2 and 3). It can be seen from these Tables that an increment in  $C_{F, in}$  does not affect the flows ( $Q_{D, in}$  and  $Q_{F, in}$ ) to obtain  $PD_{id, max}$  and  $P_{TB, max}$ , but does affect  $p_{D, in}$  and  $R$ . The higher  $C_{F, in}$ , the lower  $p_{D, in}$  and  $R$ .

### 3.2. Impact of $C_{D, in}$

Different values for  $C_{D, in}$ , with  $C_{F, in}$  and  $p_{F, in}$  fixed, result in changes of the operating points to obtain  $PD_{id, max}$ . This can be seen from the comparison of Tables 2, 4 and 5. These tables show the operating points to obtain  $PD_{id, max}$  and  $P_{TB, max}$  with  $C_{D, in} = 30, 40$  and  $50 \text{ g L}^{-1}$ , respectively. In general, the higher the difference between  $C_{D, in}$  and  $C_{F, in}$ , the higher the  $p_{D, in}$ ,  $Q_{F, in}$ ,  $R$  and  $PD_{id, max}$ . Considering 8 SWMM in series, the  $Q_{D, in}$  to obtain  $PD_{id, max}$  and  $P_{TB, max}$  decreases from 15 to 14.5 m<sup>3</sup> h<sup>-1</sup> when  $C_{D, in} = 50 \text{ g L}^{-1}$  (Table 5). For  $C_{D, in} = 30$  and  $40 \text{ g L}^{-1}$ ,  $PD_{id, max}$  is obtained when 3 SWMMs are arranged in series (Tables 2 and 4). However, for  $C_{D, in} = 50 \text{ g L}^{-1}$ ,  $PD_{id, max}$  is obtained with 2 SWMMs in series (Table 5). This is because increasing the difference between  $C_{D, in}$  and  $C_{F, in}$  makes  $\Delta\pi$  to increase and this allow to increase  $PD_{id, max}$  with less  $S_m$ . These results show that the operating points for  $PD_{id, max}$  change depending on the number of SWMMs arranged in series.

### 3.3. Impact of $p_{F, in}$ and $p_{D, in}$

A membrane based pre-treatment or cartridge filter may cause  $p_{F, in}$  variation due to fouling. This affects  $PD_{id, max}$  and  $P_{TB, max}$ . The highest values were found to be 1.74 W m<sup>-2</sup> and 203.17 W for  $PD_{id, max}$  and  $P_{TB, max}$ , respectively. Comparing Figs. 4 and 6, it can be seen how  $PD_{id, max}$  and  $P_{TB, max}$  increase with the same SWMMs in series. An increment of 1 bar in  $p_{F, in}$  causes an increase of 0.14 W m<sup>-2</sup> and 16 W for the highest values of  $PD_{id, max}$  and  $P_{TB, max}$ , respectively. As with variations of  $C_{F, in}$ , higher values of  $p_{F, in}$  affect  $p_{D, in}$  and  $R$ , with higher operating point values for both (Table 6).

For fixed values of  $C_{D, in}$ ,  $C_{F, in}$  and  $p_{F, in}$  multiple operating points for each value of  $p_{D, in}$  are obtained by changing the flows ( $Q_{D, in}$  and  $Q_{F, in}$ ). Fig. 7 shows the  $P_{TB}$  for different values of  $p_{D, in}$  and considering  $C_{D, in} = 40 \text{ g L}^{-1}$ ,  $C_{F, in} = 0.5 \text{ g L}^{-1}$  and  $p_{F, in} = 2$  bar. Different values for  $Q_{D, in}$  and  $Q_{F, in}$  at  $p_{D, in} = 1.90 \text{ MPa}$  caused  $P_{TB}$  to vary from around 212 to 299 W. This underlines the importance of controlling the flows on both the draw and feed sides, as well as other operating parameters. The maximum value of  $P_{TB}$  is 299.48 W and was found for  $p_{D, in} = 1.90 \text{ MPa}$ ,  $Q_{D, in} = 15 \text{ m}^3 \text{ h}^{-1}$ ,  $Q_{F, in} = 5.5 \text{ m}^3 \text{ h}^{-1}$  and  $R = 14.75\%$ . This operating point did not have the highest  $R$  or  $Q_p$ , as can be seen in Fig. 8. This is because  $p_{D, out}$  decreases with higher  $Q_p$  as the result of the pressure drop increment on the draw side. As expected,  $Q_p$  values decreased with higher  $p_{D, in}$  values. The maximum value of  $Q_p$  was 1.63 m<sup>3</sup> h<sup>-1</sup> and the operating point to obtain maximum  $P_{TB}$  had a  $Q_p$  value of about 0.81 m<sup>3</sup> h<sup>-1</sup>.

Fig. 9 shows the variation of  $P_{TB}$  with  $p_{F, in}$  and  $p_{D, in}$  considering 8 SWMMs in series,  $C_{D, in} = 60 \text{ g L}^{-1}$ ,  $C_{F, in} = 0.5 \text{ g L}^{-1}$ ,  $Q_{F, in} = 14.5 \text{ m}^3 \text{ h}^{-1}$  and  $Q_{D, in} = 7.5 \text{ m}^3 \text{ h}^{-1}$ . It is clear that the higher the  $p_{F, in}$  the higher the  $P_{TB}$ , but also the higher the energy consumed by the feed

**Table 2**  
Operating points for  $PD_{id, max}$  and  $P_{TB, max}$  with  $C_{D, in}=30 \text{ g L}^{-1}$ ,  $C_{F, in}=0.5 \text{ g L}^{-1}$  and  $p_{F, in}=2$  bar.

Parameter	SWMMs in series							
	1	2	3	4	5	6	7	8
$p_{D, in}$ (MPa)	1.25	1.50	1.55	1.55	1.55	1.50	1.50	1.50
$Q_{D, in}$ (m <sup>3</sup> h <sup>-1</sup> )	8	15.5	15.5	15.5	15.5	15	15	15
$Q_{F, in}$ (m <sup>3</sup> h <sup>-1</sup> )	3.5	3.5	3.5	4	4	4.5	4.5	5
$R$ (%)	2.46	5.05	7.38	8.60	10.67	11.49	13.24	13.46
$PD_{id, max}$ (W m <sup>-2</sup> )	1.50	1.58	1.60	1.60	1.58	1.55	1.53	1.51

pump.  $p_{F, in}$  can vary due to the pressure drop of the feedwater pre-treatment. However, for  $C_{D, in} = 60 \text{ g L}^{-1}$ , high  $P_{TB}$  values were found in a range of 2.2–3.6 MPa for  $p_{D, in}$ . The values of this range strongly depend on the  $C_{D, in}$ .

### 3.4. Impact of $Q_{F, in}$ and $Q_{D, in}$

Fig. 10 shows  $R$  for ranges of  $Q_{D, in}$ ,  $Q_{F, in}$  and fixed  $C_{D, in}$ ,  $C_{F, in}$ ,  $p_{D, in}$  and  $p_{F, in}$ . It can be observed that the relation between the flows and  $R$  is linear and high values of  $R$  are found when  $Q_{F, in}$  is lower than values of  $Q_{D, in}$ . The maximum value of  $R$  was 26.49 % with  $Q_{D, in} = 14.9 \text{ m}^3 \text{ h}^{-1}$  and  $Q_{F, in} = 3.1 \text{ m}^3 \text{ h}^{-1}$ . However, this operating point did not provide the maximum  $Q_p$ , the value of which was 1.08 m<sup>3</sup> h<sup>-1</sup> ( $R = 14.34\%$ ) obtained with  $Q_{D, in} = 14.7 \text{ m}^3 \text{ h}^{-1}$  and  $Q_{F, in} = 7.5 \text{ m}^3 \text{ h}^{-1}$ .

$P_{TB}$  variation with  $Q_{D, in}$  and  $Q_{F, in}$  is shown in Fig. 11. It can be seen that high values of  $P_{TB}$  are found when values of  $Q_{D, in}$  and  $Q_{F, in}$  are also high. The area for high values of  $P_{TB}$  coincides with the operating points for which there are high values of  $Q_p$ . Maximum  $P_{TB}$  was 582.29 W for  $Q_{D, in} = 14.7 \text{ m}^3 \text{ h}^{-1}$  and  $Q_{F, in} = 7.3 \text{ m}^3 \text{ h}^{-1}$ . For fixed  $C_{D, in}$ ,  $C_{F, in}$ ,  $p_{D, in}$  and  $p_{F, in}$ ,  $P_{TB}$  was in a range of 404–582 W. This makes controlling flows as well as pressures crucial to maximizing energy production through the PRO system.

## 4. Conclusions

This study proposes a PRO system simulator that allows the user to estimate the performance and SOWs of full-scale systems. The user can evaluate the performance by introducing module characteristics such as permeability coefficients, active area, porosity, etc. This enables the simulation of any generic single-stage PRO system with SWMM or HF modules. The simulator allows to determine the safe operating windows as well as the optimal operating points to maximize energy generation for fixed and variable operating conditions. This can help to estimate the PRO module characteristics that are required for the PRO process to be viable. Controlling pressures and flows taking into consideration the draw and feed solution concentrations is crucial to optimize the PRO process. More information about operating ranges considering fouling indexes (such as the silt density index or membrane fouling index) should be provided by PRO membrane manufacturers in order to estimate results close to real operating conditions.

In future studies, different membrane characteristics in terms of permeability coefficients as well as the energy balance including pumps and ERD performance should be considered in order to estimate the energy generation potential of full-scale PRO plants with the current state of technology and to identify the main limiting factors. Consideration also needs to be given to a 2-stage configuration that would allow to increase the permeate flow without exceeding the limiting operating conditions. Performance decline of PRO membrane modules due to fouling should also be considered in future studies to assess the viability of the process.

### CRediT authorship contribution statement

**A. Ruiz-García:** Conceptualization, Methodology, Data curation, Writing- Original draft preparation, Visualization, Investigation,

**Table 3**  
Operating points for  $PD_{id, max}$  and  $P_{TB, max}$  with  $C_{D, in}=30 \text{ g L}^{-1}$ ,  $C_{F, in}=2.5 \text{ g L}^{-1}$  and  $p_{F, in}=2 \text{ bar}$ .

Parameter	SWMMs in series							
	1	2	3	4	5	6	7	8
$p_{D, in}$ (MPa)	1.2	1.45	1.45	1.45	1.45	1.45	1.45	1.45
$Q_{D, in}$ ( $\text{m}^3 \text{ h}^{-1}$ )	8	15.5	15.5	15.5	15.5	15	15	15
$Q_{F, in}$ ( $\text{m}^3 \text{ h}^{-1}$ )	3.5	3.5	3.5	4	4	4.5	4.5	5
R (%)	2.22	4.54	6.93	8.07	10	10.31	11.88	12.07
$PD_{id, max}$ ( $\text{W m}^{-2}$ )	1.29	1.36	1.38	1.38	1.36	1.33	1.31	1.29

**Table 4**  
Operating points for  $PD_{id, max}$  and  $P_{TB, max}$  with  $C_{D, in}=40 \text{ g L}^{-1}$ ,  $C_{F, in}=0.5 \text{ g L}^{-1}$  and  $p_{F, in}=2 \text{ bar}$ .

Parameter	SWMMs in series							
	1	2	3	4	5	6	7	8
$p_{D, in}$ (MPa)	1.7	1.9	1.95	1.9	1.9	1.9	1.9	1.9
$Q_{D, in}$ ( $\text{m}^3 \text{ h}^{-1}$ )	10.5	15.5	15.5	15.5	15	15	15	15
$Q_{F, in}$ ( $\text{m}^3 \text{ h}^{-1}$ )	4	4	4.5	4.5	5	5	5.5	5.5
R (%)	2.66	5.44	7.3	9.36	10.56	12.5	13.09	14.75
$PD_{id, max}$ ( $\text{W m}^{-2}$ )	1.20	2.31	2.32	2.29	2.25	2.21	2.18	2.14

**Table 5**  
Operating points for  $PD_{id, max}$  and  $P_{TB, max}$  with  $C_{D, in}=50 \text{ g L}^{-1}$ ,  $C_{F, in}=0.5 \text{ g L}^{-1}$  and  $p_{F, in}=2 \text{ bar}$ .

Parameter	SWMMs in series							
	1	2	3	4	5	6	7	8
$p_{D, in}$ (MPa)	2.15	2.3	2.3	2.3	2.3	2.3	2.3	2.25
$Q_{D, in}$ ( $\text{m}^3 \text{ h}^{-1}$ )	12.5	15.5	15.5	15	15	15	15	14.5
$Q_{F, in}$ ( $\text{m}^3 \text{ h}^{-1}$ )	4.5	4.5	5	5.5	5.5	6	6.5	6.5
R (%)	2.79	5.68	7.66	9.06	11.17	12.1	12.85	14.62
$PD_{id, max}$ ( $\text{W m}^{-2}$ )	3.65	3.80	3.78	3.72	3.66	3.60	3.54	3.46

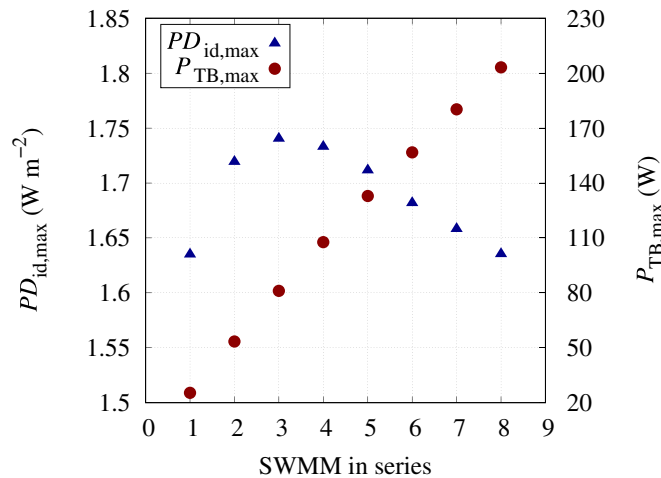


**Fig. 6.**  $PD_{id, max}$  and  $P_{TB, max}$  for 1 to 8 SWMMs in series,  $C_{D, in}=30 \text{ g L}^{-1}$ ,  $C_{F, in}=0.5 \text{ g L}^{-1}$  and  $p_{F, in}=3 \text{ bar}$ .

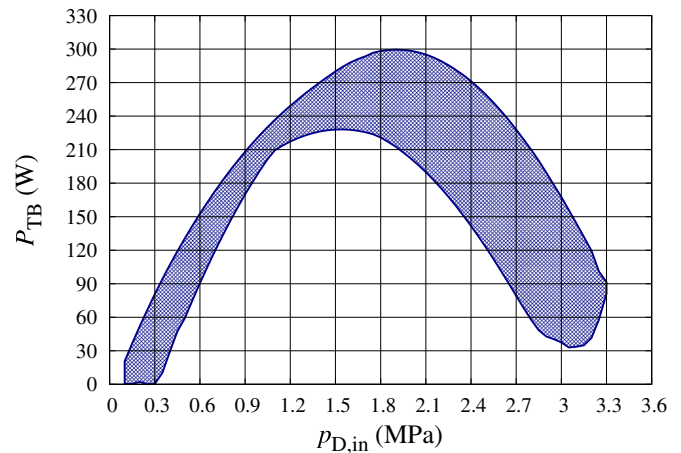


**Fig. 7.**  $P_{TB}$  for 8 SWMMs in series,  $C_{D, in}=40 \text{ g L}^{-1}$ ,  $C_{F, in}=0.5 \text{ g L}^{-1}$  and  $p_{F, in}=2 \text{ bar}$ .

**Table 6**  
Operating points for  $PD_{id, max}$  and  $P_{TB, max}$  with  $C_{D, in}=30 \text{ g L}^{-1}$ ,  $C_{F, in}=0.5 \text{ g L}^{-1}$  and  $p_{F, in}=3 \text{ bar}$ .

Parameter	SWMMs in series							
	1	2	3	4	5	6	7	8
$p_{D, in}$ (MPa)	1.35	1.55	1.60	1.60	1.65	1.55	1.55	1.55
$Q_{D, in}$ ( $\text{m}^3 \text{ h}^{-1}$ )	8.5	15.5	15.5	15.5	15.5	15	15	15
$Q_{F, in}$ ( $\text{m}^3 \text{ h}^{-1}$ )	3.5	3.5	3.5	4	4	4.5	4.5	5
R (%)	2.49	5.26	7.70	8.96	10.67	11.96	13.79	14.03

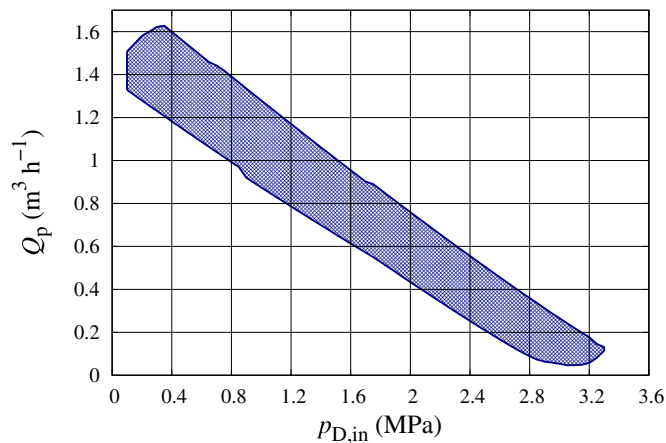


Fig. 8.  $Q_p$  for 8 SWMMs in series,  $C_{D, in}=40 \text{ g L}^{-1}$ ,  $C_{F, in}=0.5 \text{ g L}^{-1}$  and  $p_{F, in}=2 \text{ bar}$ .

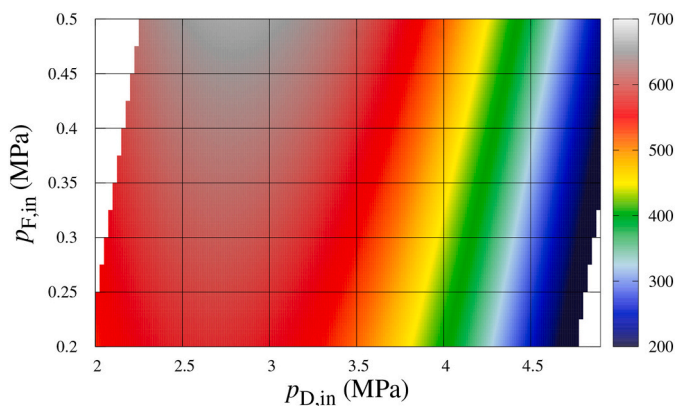


Fig. 9.  $P_{TB}$  for 8 SWMMs in series,  $C_{D, in}=60 \text{ g L}^{-1}$ ,  $C_{F, in}=0.5 \text{ g L}^{-1}$ ,  $Q_{F, in}=14.5 \text{ m}^3 \text{ h}^{-1}$  and  $Q_{D, in}=7.5 \text{ m}^3 \text{ h}^{-1}$ .

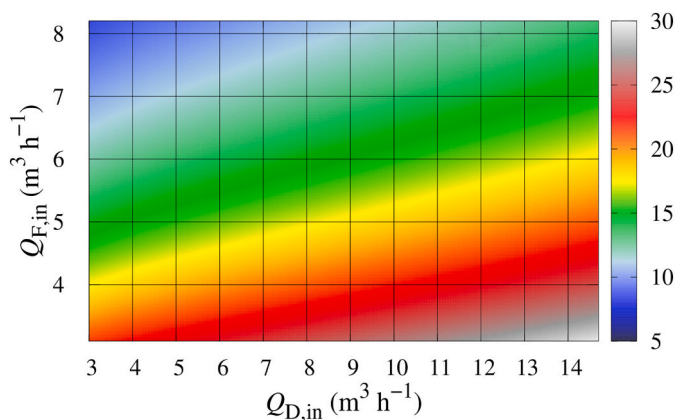


Fig. 10.  $R$  for 8 SWMMs in series,  $C_{D, in}=60 \text{ g L}^{-1}$ ,  $C_{F, in}=0.5 \text{ g L}^{-1}$ ,  $p_{D, in}=26.5 \text{ bar}$  and  $p_{F, in}=2 \text{ bar}$ .

Validation, Writing- Reviewing and Editing.

I. Nuez: Conceptualization, Resources, Supervision.

F. Tadeo: Conceptualization, Resources, Supervision.

**Declaration of competing interest**

The authors declare that they have no known competing financial interests or personal relationships that could have appeared to influence

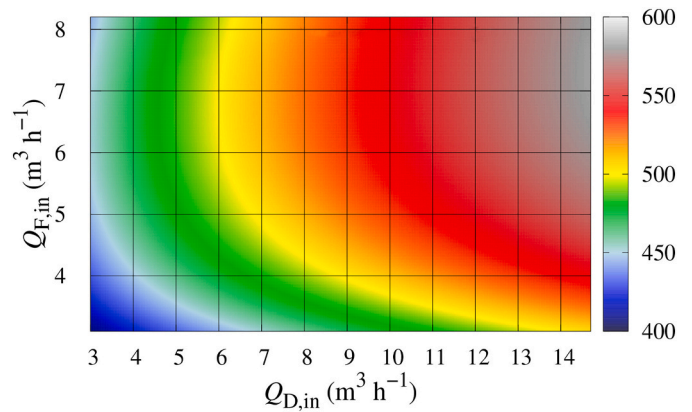


Fig. 11.  $P_{TB}$  for 8 SWMMs in series,  $C_{D, in}=60 \text{ g L}^{-1}$ ,  $C_{F, in}=0.5 \text{ g L}^{-1}$ ,  $p_{D, in}=26.5 \text{ bar}$  and  $p_{F, in}=2 \text{ bar}$ .

the work reported in this paper.

**Data availability**

No data was used for the research described in the article.

**Acknowledgements**

This research was co-funded by the ERDF and the ACLIEMAC Project (MAC2/3.5b/380) of the INTERREG V-A MAC 2014-2020 program.

**References**

- [1] R.H. Moss, J.A. Edmonds, K.A. Hibbard, M.R. Manning, S.K. Rose, D.P. Van Vuuren, T.R. Carter, S. Emori, M. Kainuma, T. Kram, et al., The next generation of scenarios for climate change research and assessment, *Nature* 463 (7282) (2010) 747–756.
- [2] B. Kruyt, D. van Vuuren, H. de Vries, H. Groenoberg, Indicators for energy security, *Energy Policy* 37 (6) (2009) 2166–2181, <https://doi.org/10.1016/j.enpol.2009.02.006>, china Energy Efficiency.
- [3] R.R. Gonzales, A. Abdel-Wahab, S. Adham, D.S. Han, S. Phuntsho, W. Suwaileh, N. Hilal, H.K. Shon, Salinity gradient energy generation by pressure retarded osmosis: a review, *Desalination* 500 (2021), 114841, <https://doi.org/10.1016/j.desal.2020.114841>.
- [4] M. Tawalbeh, A. Al-Othman, N. Abdelwahab, A.H. Alami, A.G. Olabi, Recent developments in pressure retarded osmosis for desalination and power generation, *Renew. Sust. Energ. Rev.* 138 (2021), 110492, <https://doi.org/10.1016/j.rser.2020.110492>.
- [5] Y. Jiao, L. Song, C. Zhao, Y. An, W. Lu, B. He, C. Yang, Membrane-based indirect power generation technologies for harvesting salinity gradient energy - a review, *Desalination* 525 (2022), 115485, <https://doi.org/10.1016/j.desal.2021.115485>.
- [6] A.P. Straub, A. Deshmukh, M. Elimelech, Pressure-retarded osmosis for power generation from salinity gradients: is it viable? *Energy Environ. Sci.* 9 (2016) 31–48, <https://doi.org/10.1039/C5EE02985F>.
- [7] N.Y. Yip, M. Elimelech, Comparison of energy efficiency and power density in pressure retarded osmosis and reverse electrodialysis, *Environ. Sci. Technol.* 48 (18) (2014) 11002–11012, <https://doi.org/10.1021/es5029316>, PMID: 25157687. arXiv:doi:10.1021/es5029316.
- [8] C. Lee, S.H. Chae, E. Yang, S. Kim, J.H. Kim, I.S. Kim, A comprehensive review of the feasibility of pressure retarded osmosis: recent technological advances and industrial efforts towards commercialization, *Desalination* 491 (2020), 114501, <https://doi.org/10.1016/j.desal.2020.114501>.
- [9] M. Kishimoto, Y. Tanaka, M. Yasukawa, S. Goda, M. Higa, H. Matsuyama, Optimization of pressure-retarded osmosis with hollow-fiber membrane modules by numerical simulation, *Ind. Eng. Chem. Res.* 58 (16) (2019) 6687–6695, <https://doi.org/10.1021/acs.iecr.9b00139>, arXiv:doi:10.1021/acs.iecr.9b00139.
- [10] K. Touati, F. Tadeo, Study of the reverse salt diffusion in pressure retarded osmosis: influence on concentration polarization and effect of the operating conditions, *Desalination* 389 (2016) 171–186, <https://doi.org/10.1016/j.desal.2016.02.014>, pressure Retarded Osmosis.
- [11] A.P. Straub, S. Lin, M. Elimelech, Module-scale analysis of pressure retarded osmosis: performance limitations and implications for full-scale operation, *Environ. Sci. Technol.* 48 (20) (2014) 12435–12444, <https://doi.org/10.1021/es503790k>, PMID: 25222561. arXiv:doi:10.1021/es503790k.
- [12] N. AlZainati, H. Saleem, A. Altaee, S.J. Zaidi, M. Mohsen, A. Hawari, G.J. Millar, Pressure retarded osmosis: advancement, challenges and potential, *J. Water Process. Eng.* 40 (2021), 101950, <https://doi.org/10.1016/j.jwpe.2021.101950>.

- [13] Y. Tanaka, M. Yasukawa, S. Goda, H. Sakurai, M. Shibuya, T. Takahashi, M. Kishimoto, M. Higa, H. Matsuyama, Experimental and simulation studies of two types of 5-inch scale hollow fiber membrane modules for pressure-retarded osmosis, *Desalination* 447 (2018) 133–146, <https://doi.org/10.1016/j.desal.2018.09.015>.
- [14] J. Benjamin, S.A.L. Mashrafi, A. Tejada-Martinez, N. Diaz-Elsayed, M.E. Arias, Q. Zhang, Optimizing pressure retarded osmosis spacer geometries: an experimental and CFD modeling study, *J. Membr. Sci.* 647 (2022), 120284, <https://doi.org/10.1016/j.memsci.2022.120284>.
- [15] N.A. Pham, D.Y.F. Ng, K. Goh, Z. Dong, R. Wang, Assessing the potential of integrally skinned asymmetric hollow fiber membranes for addressing membrane fouling in pressure retarded osmosis process, *Desalination* 520 (2021), 115347, <https://doi.org/10.1016/j.desal.2021.115347>.
- [16] J. Ju, Y. Choi, S. Lee, N. Jeong, Comparison of fouling characteristics between reverse electro dialysis (RED) and pressure retarded osmosis (PRO), *Desalination* 497 (2021), 114648, <https://doi.org/10.1016/j.desal.2020.114648>.
- [17] S.L. Plata, A.E. Childress, Limiting power density in pressure-retarded osmosis: observation and implications, *Desalination* 467 (2019) 51–56, <https://doi.org/10.1016/j.desal.2019.05.013>.
- [18] W.R. Thelin, E. Sivertsen, T. Holt, G. Brekke, Natural organic matter fouling in pressure retarded osmosis, *J. Membr. Sci.* 438 (2013) 46–56, <https://doi.org/10.1016/j.memsci.2013.03.020>.
- [19] Q. She, Y.K.W. Wong, S. Zhao, C.Y. Tang, Organic fouling in pressure retarded osmosis: experiments, mechanisms and implications, *J. Membr. Sci.* 428 (2013) 181–189, <https://doi.org/10.1016/j.memsci.2012.10.045>.
- [20] J.A. Idarraga-Mora, A.D. O'Neal, M.E. Pfeiler, D.A. Ladner, S.M. Husson, Effect of mechanical strain on the transport properties of thin-film composite membranes used in osmotic processes, *J. Membr. Sci.* 615 (2020), 118488, <https://doi.org/10.1016/j.memsci.2020.118488>.
- [21] Z.L. Cheng, T.-S. Chung, Mass transport of various membrane configurations in pressure retarded osmosis (PRO), *J. Membr. Sci.* 537 (2017) 160–176, <https://doi.org/10.1016/j.memsci.2017.05.008>.
- [22] R.R. Gonzales, Y. Yang, M.J. Park, T.-H. Bae, A. Abdel-Wahab, S. Phuntsho, H. K. Shon, Enhanced water permeability and osmotic power generation with sulfonate-functionalized porous polymer-incorporated thin film nanocomposite membranes, *Desalination* 496 (2020), 114756, <https://doi.org/10.1016/j.desal.2020.114756>.
- [23] X. Liu, L.-X. Foo, Y. Li, J.-Y. Lee, B. Cao, C.Y. Tang, Fabrication and characterization of nanocomposite pressure retarded osmosis (pro) membranes with excellent anti-biofouling property and enhanced water permeability, *Desalination* 389 (2016) 137–148, <https://doi.org/10.1016/j.desal.2016.01.037>, pressure Retarded Osmosis.
- [24] S. Zhang, T.-S. Chung, Minimizing the instant and accumulative effects of salt permeability to sustain ultrahigh osmotic power density, *Environ. Sci. Technol.* 47 (17) (2013) 10085–10092, <https://doi.org/10.1021/es402690v>, PMID: 23941367, arXiv:doi:10.1021/es402690v.
- [25] C.D. Peters, D.Y.F. Ng, N.P. Hankins, Q. She, A novel method for the accurate characterization of transport and structural parameters of deformable membranes utilized in pressure- and osmotically driven membrane processes, *J. Membr. Sci.* 638 (2021), 119720, <https://doi.org/10.1016/j.memsci.2021.119720>.
- [26] N.-N. Bui, J.T. Arena, J.R. McCutcheon, Proper accounting of mass transfer resistances in forward osmosis: improving the accuracy of model predictions of structural parameter, *J. Membr. Sci.* 492 (2015) 289–302, <https://doi.org/10.1016/j.memsci.2015.02.001>.
- [27] T.-S. Chung, C.F. Wan, *Membrane Technology for Osmotic Power Generation by Pressure Retarded Osmosis*, CRC Press, 2020.
- [28] A. Ruiz-García I. Nuez, Performance assessment of SWRO spiral-wound membrane modules with different feed spacer dimensions, *Processes* 8 (6). doi:10.3390/pr8060692.
- [29] J. Sim, J. Koo, S. Nam, E. Kim, T. Hwang, et al., Effect of combined positions of feed spacer-type tricot on the performance in pressure retarded osmosis (PRO), *Desalin. Water Treat.* 77 (2017) 63–68.
- [30] K.L. Hickenbottom, J. Vanneste, M. Elimelech, T.Y. Cath, Assessing the current state of commercially available membranes and spacers for energy production with pressure retarded osmosis, *Desalination* 389 (2016) 108–118, <https://doi.org/10.1016/j.desal.2015.09.029>, pressure Retarded Osmosis.
- [31] Q. She, D. Hou, J. Liu, K.H. Tan, C.Y. Tang, Effect of feed spacer induced membrane deformation on the performance of pressure retarded osmosis (PRO): implications for PRO process operation, *J. Membr. Sci.* 445 (2013) 170–182, <https://doi.org/10.1016/j.memsci.2013.05.061>.
- [32] Y.C. Kim, M. Elimelech, Adverse impact of feed channel spacers on the performance of pressure retarded osmosis, *Environ. Sci. Technol.* 46 (8) (2012) 4673–4681, <https://doi.org/10.1021/es3002597>, PMID: 22420537, arXiv:doi:10.1021/es3002597.
- [33] Y.C. Kim, M. Elimelech, Potential of osmotic power generation by pressure retarded osmosis using seawater as feed solution: analysis and experiments, *J. Membr. Sci.* 429 (2013) 330–337, <https://doi.org/10.1016/j.memsci.2012.11.039>.
- [34] Y. Shi, M. Zhang, H. Zhang, F. Yang, C.Y. Tang, Y. Dong, Recent development of pressure retarded osmosis membranes for water and energy sustainability: a critical review, *Water Res.* 189 (2021), 116666, <https://doi.org/10.1016/j.watres.2020.116666>.
- [35] A. Achilli, T.Y. Cath, A.E. Childress, Power generation with pressure retarded osmosis: an experimental and theoretical investigation, *J. Membr. Sci.* 343 (1) (2009) 42–52, <https://doi.org/10.1016/j.memsci.2009.07.006>.
- [36] A. Achilli, A.E. Childress, Pressure retarded osmosis: from the vision of Sidney Loeb to the first prototype installation — review, *Desalination* 261 (3) (2010) 205–211, <https://doi.org/10.1016/j.desal.2010.06.017>, PMID: 22420537, arXiv:doi:10.1021/es3002597.
- [37] J. Kim, M. Park, S.A. Snyder, J.H. Kim, Reverse osmosis (RO) and pressure retarded osmosis (PRO) hybrid processes: model-based scenario study, *Desalination* 322 (2013) 121–130, <https://doi.org/10.1016/j.desal.2013.05.010>.
- [38] C.F. Wan, T.-S. Chung, Energy recovery by pressure retarded osmosis (PRO) in SWRO-PRO integrated processes, *Appl. Energy* 162 (2016) 687–698, <https://doi.org/10.1016/j.apenergy.2015.10.067>.
- [39] E. Bargiacchi, F. Orciuolo, L. Ferrari, U. Desideri, Use of pressure-retarded-osmosis to reduce reverse osmosis energy consumption by exploiting hypersaline flows, *Energy* 211 (2020), 118969, <https://doi.org/10.1016/j.energy.2020.118969>.
- [40] B. Blankert, Y. Kim, H. Vrouwenvelder, N. Ghaffour, Facultative hybrid ro-pro concept to improve economic performance of pro: feasibility and maximizing efficiency, *Desalination* 478 (2020), 114268, <https://doi.org/10.1016/j.desal.2019.114268>.
- [41] Z.M. Binger, A. Achilli, Forward osmosis and pressure retarded osmosis process modeling for integration with seawater reverse osmosis desalination, *Desalination* 491 (2020), 114583, <https://doi.org/10.1016/j.desal.2020.114583>.
- [42] A. Altaee, N. Hilal, Dual-stage forward osmosis/pressure retarded osmosis process for hypersaline solutions and fracking wastewater treatment, *Desalination* 350 (2014) 79–85, <https://doi.org/10.1016/j.desal.2014.07.013>.
- [43] Z.L. Cheng, X. Li, T.-S. Chung, The forward osmosis-pressure retarded osmosis (FO-PRO) hybrid system: a new process to mitigate membrane fouling for sustainable osmotic power generation, *J. Membr. Sci.* 559 (2018) 63–74, <https://doi.org/10.1016/j.memsci.2018.04.036>.
- [44] A. Altaee, A. Sharif, G. Zaragoza, A.F. Ismail, Evaluation of FO-RO and PRO-RO designs for power generation and seawater desalination using impaired water feeds, *Desalination* 368 (2015) 27–35, <https://doi.org/10.1016/j.desal.2014.06.022>, reverse Osmosis.
- [45] S. Lin, N.Y. Yip, T.Y. Cath, C.O. Osuji, M. Elimelech, Hybrid pressure retarded osmosis-membrane distillation system for power generation from low-grade heat: thermodynamic analysis and energy efficiency, *Environ. Sci. Technol.* 48 (9) (2014) 5306–5313, <https://doi.org/10.1021/es405173b>, PMID: 24724732, arXiv:doi:10.1021/es405173b.
- [46] S.J. Moon, S.M. Jeon, J.H. Kim, Y.M. Lee, Membrane distillation & pressure retarded osmosis hybrid system using thermally rearranged nanofibrous membranes, *J. Membr. Sci.* 638 (2021), 119735, <https://doi.org/10.1016/j.memsci.2021.119735>.
- [47] J.T. Arena, K.K. Reimund, J.R. McCutcheon, On the importance of selectivity and support layer compaction in pressure retarded osmosis, *Desalination* 498 (2021), 114804, <https://doi.org/10.1016/j.desal.2020.114804>.
- [48] Y. Chen, C.H. Loh, L. Zhang, L. Setiawan, Q. She, W. Fang, X. Hu, R. Wang, Module scale-up and performance evaluation of thin film composite hollow fiber membranes for pressure retarded osmosis, *J. Membr. Sci.* 548 (2018) 398–407, <https://doi.org/10.1016/j.memsci.2017.11.036>.
- [49] M. Zhang, D. Hou, Q. She, C.Y. Tang, Gypsum scaling in pressure retarded osmosis: experiments, mechanisms and implications, *Water Res.* 48 (2014) 387–395, <https://doi.org/10.1016/j.watres.2013.09.051>.
- [50] P.-F. Sun, Y. Jang, S.-Y. Ham, H. Ryoo, H.-D. Park, Effects of reverse solute diffusion on membrane biofouling in pressure-retarded osmosis processes, *Desalination* 512 (2021), 115145, <https://doi.org/10.1016/j.desal.2021.115145>.
- [51] J. Fei, W. Mai, P.S. Cheng, J. Shi, Z. Liu, Q. She, Membrane structure-dependent limiting flux behavior and membrane selectivity loss during gypsum scaling: implications for pressure-retarded osmosis operation and membrane design, *Desalination* 492 (2020), 114644, <https://doi.org/10.1016/j.desal.2020.114644>.
- [52] Y. Xu, X. Peng, C.Y. Tang, Q.S. Fu, S. Nie, Effect of draw solution concentration and operating conditions on forward osmosis and pressure retarded osmosis performance in a spiral wound module, *J. Membr. Sci.* 348 (1) (2010) 298–309, <https://doi.org/10.1016/j.memsci.2009.11.013>.
- [53] S. Chou, R. Wang, L. Shi, Q. She, C. Tang, A.G. Fane, Thin-film composite hollow fiber membranes for pressure retarded osmosis (PRO) process with high power density, *J. Membr. Sci.* 389 (2012) 25–33, <https://doi.org/10.1016/j.memsci.2011.10.002>.
- [54] D. Attarde, M. Jain, K. Chaudhary, S.K. Gupta, Osmotically driven membrane processes by using a spiral wound module — modeling, experimentation and numerical parameter estimation, *Desalination* 361 (2015) 81–94, <https://doi.org/10.1016/j.desal.2015.01.025>.
- [55] S. Lee, Y.C. Kim, S.-J. Park, S.-K. Lee, H.-C. Choi, Experiment and modeling for performance of a spiral-wound pressure-retarded osmosis membrane module, *Desalin. Water Treat.* 57 (22) (2016) 10101–10110, <https://doi.org/10.1080/19443994.2015.1043494>, arXiv:doi:10.1080/19443994.2015.1043494.
- [56] G. O'Toole, L. Jones, C. Coutinho, C. Hayes, M. Naples, A. Achilli, River-to-sea pressure retarded osmosis: resource utilization in a full-scale facility, *Desalination* 389 (2016) 39–51, <https://doi.org/10.1016/j.desal.2016.01.012>, arXiv:doi:10.1021/aes.iecr.9b00139.
- [57] A. Achilli, J.L. Prante, N.T. Hancock, E.B. Maxwell, A.E. Childress, Experimental results from RO-PRO: a next generation system for low-energy desalination, PMID: 24798068, *Environ. Sci. Technol.* 48 (11) (2014) 6437–6443, <https://doi.org/10.1021/es405556s>, arXiv:doi:10.1021/es405556s.
- [58] M. Higa, D. Shigefuji, M. Shibuya, S. Izumikawa, Y. Ikebe, M. Yasukawa, N. Endo, A. Tanioka, Experimental study of a hollow fiber membrane module in pressure-retarded osmosis: module performance comparison with volumetric-based power outputs, *Desalination* 420 (2017) 45–53, <https://doi.org/10.1016/j.desal.2017.06.015>.

- [59] Y. Chen, A.A. Alanezi, J. Zhou, A. Altaee, M.H. Shaheed, Optimization of module pressure retarded osmosis membrane for maximum energy extraction, *J. Water Process. Eng.* 32 (2019), 100935, <https://doi.org/10.1016/j.jwpe.2019.100935>.
- [60] K. Saito, M. Irie, S. Zaito, H. Sakai, H. Hayashi, A. Tanioka, Power generation with salinity gradient by pressure retarded osmosis using concentrated brine from SWRO system and treated sewage as pure water, *Desalin. Water Treat.* 41 (1-3) (2012) 114–121, <https://doi.org/10.1080/19443994.2012.664696>, arXiv:doi:10.1080/19443994.2012.664696.
- [61] A.O. Sharif, A.A. Merdaw, M. Aryafar, P. Nicoll, Theoretical and experimental investigations of the potential of osmotic energy for power production, *Membranes* 4 (3) (2014) 447–468, <https://doi.org/10.3390/membranes4030447>.
- [62] A.N. Newby, T.V. Bartholomew, M.S. Mauter, The economic infeasibility of salinity gradient energy via pressure retarded osmosis, *ACS ES&T Eng.* 1 (7) (2021) 1113–1121, <https://doi.org/10.1021/acsestengg.1c00078>, arXiv:doi:10.1021/acsestengg.1c00078.
- [63] H.W. Chung, J. Swaminathan, L.D. Banchik, J.H. Lienhard, Economic framework for net power density and leveled cost of electricity in pressure-retarded osmosis, *Desalination* 448 (2018) 13–20, <https://doi.org/10.1016/j.desal.2018.09.007>.
- [64] H.T. Madsen, T. Bruun Hansen, T. Nakao, S. Goda, E.G. Sogaard, Combined geothermal heat and pressure retarded osmosis as a new green power system, *Energy Convers. Manag.* 226 (2020), 113504, <https://doi.org/10.1016/j.enconman.2020.113504>.
- [65] S. Sarp, N. Hilal, Thermodynamic optimization of multistage pressure retarded osmosis (MPRO) with variable feed pressures for hypersaline solutions, *Desalination* 477 (2020), 114245, <https://doi.org/10.1016/j.desal.2019.114245>.
- [66] H.W. Chung, J. Swaminathan, J.H. Lienhard, Multistage pressure-retarded osmosis configurations: a unifying framework and thermodynamic analysis, *Desalination* 476 (2020), 114230, <https://doi.org/10.1016/j.desal.2019.114230>.
- [67] G. Schock, A. Miquel, Mass transfer and pressure loss in spiral wound modules, *Desalination* 64 (1987) 339–352, [https://doi.org/10.1016/0011-9164\(87\)90107-X](https://doi.org/10.1016/0011-9164(87)90107-X).
- [68] N.Y. Yip, A. Tiraferri, W.A. Phillip, J.D. Schiffman, L.A. Hoover, Y.C. Kim, M. Elimelech, Thin-film composite pressure retarded osmosis membranes for sustainable power generation from salinity gradients, *Environ. Sci. Technol.* 45 (10) (2011) 4360–4369, <https://doi.org/10.1021/es104325z>, PMID: 21491936, arXiv:doi:10.1021/es104325z.
- [69] S. Loeb, Production of energy from concentrated brines by pressure-retarded osmosis: I. Preliminary technical and economic correlations, *J. Membr. Sci.* 1 (1976) 49–63, [https://doi.org/10.1016/S0376-7388\(00\)82257-7](https://doi.org/10.1016/S0376-7388(00)82257-7).
- [70] K. Touati, C. Hänel, F. Tadeo, T. Schiestel, Effect of the feed and draw solution temperatures on PRO performance: theoretical and experimental study, *Desalination* 365 (2015) 182–195, <https://doi.org/10.1016/j.desal.2015.02.016>.
- [71] A. Ruiz-García, I. de la Nuez-Pestana, A computational tool for designing bwro systems with spiral wound modules, *Desalination* 426 (2018) 69–77, <https://doi.org/10.1016/j.desal.2017.10.040>.
- [72] S. Phuntsho, S. Hong, M. Elimelech, H.K. Shon, Osmotic equilibrium in the forward osmosis process: modelling, experiments and implications for process performance, *J. Membr. Sci.* 453 (2014) 240–252, <https://doi.org/10.1016/j.memsci.2013.11.009>.
- [73] K. Lee, R. Baker, H. Lonsdale, Membranes for power generation by pressure-retarded osmosis, *J. Membr. Sci.* 8 (2) (1981) 141–171, [https://doi.org/10.1016/S0376-7388\(00\)82088-8](https://doi.org/10.1016/S0376-7388(00)82088-8).
- [74] E.K. Touati, F. Tadeo, J.H. Kim, O.A.A. Silva, S.H. Chae, *Pressure Retarded Osmosis: Renewable Energy Generation and Recovery*, Academic Press, 2017.
- [75] C.H. Tan, H.Y. Ng, Revised external and internal concentration polarization models to improve flux prediction in forward osmosis process, *Desalination* 309 (2013) 125–140, <https://doi.org/10.1016/j.desal.2012.09.022>.
- [76] V. Geraldes, N.E. Pereira, M.N. de Pinho, Simulation and optimization of medium-sized seawater reverse osmosis processes with spiral-wound modules, *Ind. Eng. Chem. Res.* 44 (6) (2005) 1897–1905, <https://doi.org/10.1021/ie049357s>.
- [77] R.P. Brent, *Algorithms for Minimization Without Derivatives*, Courier Corporation, 2013.
- [78] G.E. Forsythe, M.A. Malcolm, C.B. Moler, *Computer Methods for Mathematical Computations*, Prentice-Hall, 1977.
- [79] J. Cooper R. Dooley, International Association for the Properties of Water and Steam: Release on the IAPWS Formulation 2008 for the Viscosity of Ordinary Water Substance, IAPWS Release, IAPWS Secretariat.
- [80] M.H. Sharqawy, J.H. Lienhard V, S.M. Zubair, On exergy calculations of seawater with applications in desalination systems, *Int. J. Therm. Sci.* 50 (2) (2011) 187–196, <https://doi.org/10.1016/j.ijthermalsci.2010.09.013>.